NSF Grant # 0846385
NSF PROGRAM NAME: Dynamical Systems

Dynamics of Coupled Electromagnetically-Actuated Microbeams

Vijay Kumar, Andrew Sabater and Jeffrey F. Rhoads[PI]
School of Mechanical Engineering and Birck Nanotechnology Center, Purdue University
Contact Email: jfrhoads@purdue.edu

Abstract:

Over the past decade, electromagnetically-transduced microelectromechanical systems (MEMS) have garnered significant research interest due to their scalability, self-sensing capabilities, and ease of integration with external electronics and associated hardware. The current work seeks to build upon prior efforts in this area by exploring the linear and nonlinear dynamics of coupled arrays of electromagnetically-actuated microbeams. The first portion of the work details the ongoing development of a single input - single output (SISO), multi-analyte resonant mass sensor founded upon a globally-coupled array of selectively-functionalized, electromagnetically-actuated microbeams. The latter portion of the work investigates how electromagnetically-actuated microbeams can be used in conjunction with a positive feedback loop to develop functional oscillators and associated arrays – essential components in a variety of electromechanical signal processing and computing systems.

1. Introduction:

Electromagnetically-transduced, resonant microelectromechanical systems (MEMS) have garnered significant research interest over the past decade due to their scalability, self-sensing capabilities, and ease of integration with external electronics and associated hardware [1–5]. In typical implementations, these devices consist of a flexible structure with a current-carrying wire loop patterned on its surface, which is placed in an external magnetic field. The flow of current through the current loop induces a Lorentz force, which in turn provides a tunable form of actuation. Likewise, the motion of the conductor through the magnetic field induces a response-dependent electromotive force (emf), which can be used to directly recover the response of the system, for feedback purposes, or as a basis for electromagnetic coupling in an oscillator array.

In 2006, Requa developed a class of electromagnetically-actuated microcantilever resonators which had two wire loops patterned on the device's surface: one for actuation purposes and another which was used to sense the emf resulting from the interaction between the moving coil and an external magnetic field [6–8]. Rhoads subsequently studied the behavior of these resonators accounting for large deformations and parametric excitations [9]. The present work seeks to build upon the technical understanding developed in these efforts.

Although isolated microresonators have dominated the MEMS application space, recent studies of coupled arrays have demonstrated that the rich dynamical behaviors associated with these systems can be exploited for practical gain (see, for example, [10–12]). In this spirit, the current effort also seeks to utilize the dynamic behavior of arrays of electromagnetically-actuated microbeams in the development of novel mass sensors and electromechanical signal processing and computing elements.

The use of coupled MEMS devices for mass sensing purposes has gained considerable attention since the first experimental demonstrations of this technology by Spletzer and collaborators [13, 14]. In these works, the authors showed the utility of using spatially-localized modes for the detection and identification of multiple analytes. Building upon this work, Gil-Santos and collaborators subsequently exploited the deterministic and stochastic responses of elastically-coupled cantilevers to improve the sensitivity of such systems [15]. Likewise, in an effort to decrease the hardware requirements associated with multi-analyte sensing, DeMartini, Rhoads and collaborators designed a single input - single output (SISO) sensor which utilized an array of resonators, coupled through a common shuttle mass [16, 17]. The first portion of this work investigates a refinement of this latter technology based upon an array of globally-coupled, electromagnetically-actuated microcantilevers.

In 2000, Hoppensteadt and Izhikevich proposed the use of arrays of MEMS oscillators in neurocomputing [18]. Since then, considerable effort has focused on the development of MEMS oscillators capable of

serving as clocks, reference oscillators and basic computing elements [19]. Despite this attention, comparatively little work has focused on the fabrication and implementation of coupled oscillators using MEMS devices and demonstrating the utility of synchronization in small-scale systems (though there are a number of noteworthy theoretical efforts in this area, including [20, 21]).

The accepted definition of an oscillator, or self-excited system, is a system that has a limit cycle with stable amplitude and neutrally stable phase (i.e. perturbations to the system will adjust the phase and not the amplitude) [22]. Arrays of oscillators with various forms of coupling have been studied extensively in the generic literature [18, 20, 21, 23–30], but there are still open questions in the field, specifically related to the synchronization of electromechanical arrays embedded in a multiphysics environment. The synchronization of microbeam oscillators is of interest because the conditions under which synchronization occurs are a direct reflection of the parameters of the system and can be made to be independent or dependent of the system's initial conditions. Also, while synchronization is complex, determining when a system is synchronized is relatively simple, and thus the arrays can be used for sensing, signal processing and computing, amongst other applications [18, 30].

The second portion of the work deals with the dynamics of a single electromagnetically-actuated oscillator and a two element, dissipatively-coupled oscillator array. The analysis contained herein forms the foundation for a study of the amplitude dynamics of oscillator arrays, which are often ignored, but must be considered when constructing oscillators from microscale resonators. The analysis also provides a framework to study the dynamics of larger arrays with potentially different forms of coupling and feedback.

The paper is organized as follows. Section 2 details the development of a nonlinear model capable of describing the dynamics of a single electromagnetically-actuated microcantilever. Section 3 details the application of a linearized version of this model to SISO, multi-analyte sensing. Sections 4 and 5 investigate the nonlinear model in the context of isolated and coupled microbeam oscillators respectively.

2. Modeling of a Single Electromagnetically-Actuated Microbeam:

The device considered herein is a cantilevered beam with an integrated current loop, placed in a uniform permanent magnetic field $\vec{B}$, whose orientation with respect to the vertical reference measured in the counterclockwise direction is defined by α. Figure 1 shows the beam element with the associated variables used for modeling, while Fig. 2 shows the beam in three dimensions and the orientation of the magnetic field.

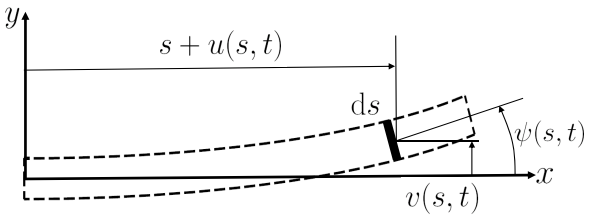

Figure 1: Schematic diagram of the beam element with a description of the variables used for modeling.

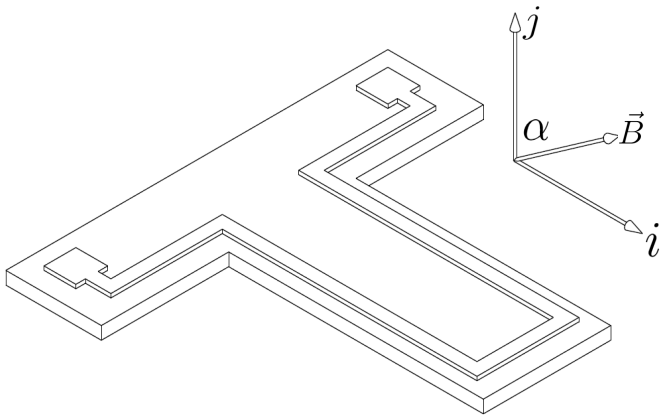

Figure 2: Model of the beam in three dimensions. The magnetic field $\vec{B}$ is oriented at an angle α with respect to the vertical reference.

Assuming that the beam has a negligible rotational inertia, the specific Lagrangian of the resonator can be defined as

$$\bar{L} = \frac{1}{2}\int_0^l \rho A\left[\dot{u}^2 + \dot{v}^2\right] \mathrm{d}s - \frac{1}{2}EI\psi'^2, \qquad (1)$$

where u, v and ψ are defined as in Fig. 1, $(\dot{\bullet})$ and $(\bullet)'$ denote the derivatives with respect to the time and the arc length variable s respectively, and ρ, A, l, E and I represent the beam's mass density, cross-sectional area, undeformed length, elastic modulus and the cross-sectional moment of inertia respectively.

Assuming that the neutral axis of the beam is inextensible and applying the extended Hamilton's principle results in the following variational equation for

the system:

$$\begin{aligned}&\delta H = 0\\&= \delta \int_{t_1}^{t_2} \int_0^l \left\{ \bar{L} + \frac{1}{2}\lambda \left[1 - (1+u')^2 - (v')^2\right] \right\} \mathrm{d}s\mathrm{d}t\\&\quad + \int_{t_1}^{t_2} \int_0^l (Q_u \delta u + Q_v \delta_v) \mathrm{d}s\mathrm{d}t,\end{aligned} \tag{2}$$

where λ is a Lagrange multiplier introduced to maintain the inextensibility constraint and Q_u and Q_v are the external non-conservative forces in the longitudinal and transverse directions respectively. Based on the geometry, the external non-conservative force in the longitudinal direction is effectively a point force at the tip and the non-conservative force in the transverse direction is a combination of the force due to damping and the electromagnetic point force at the tip:

$$\begin{aligned}Q_u &= F_1 \delta(s-l),\\Q_v &= -c\dot{v} + F_2 \delta(s-l).\end{aligned} \tag{3}$$

Here, c is a specific viscous damping coefficient and F_1 and F_2 are the external loads resulting from the Lorentz force acting on the beam in the longitudinal and transverse directions respectively. Using a third-order Taylor series approximation for ψ and integrating Eqn. (2) successively by parts yields the equations governing the longitudinal and transverse vibrations of the system.

Solving for the Lagrange multiplier in the equation for longitudinal vibrations and substituting it in the equation for the transverse vibration, along with the expression for u resulting from the inextensibility constraint, yields a single equation governing the transverse vibrations of the system. This equation is nondimensionalized to reduce the number of free parameters by introducing a scaling of the displacement, arc length and time variables as follows:

$$\hat{v} = \frac{v}{v_0}, \quad \hat{s} = \frac{s}{l}, \quad \hat{t} = \frac{t}{T}. \tag{4}$$

Here, v_0 is a characteristic displacement of the system (the beam's thickness or width), and

$$T = \sqrt{\frac{\rho A l^4}{EI}}, \quad \hat{c} = \frac{cT}{\rho A}.$$

This yields a scaled distributed-parameter model for the system as below.

$$\begin{aligned}&\frac{\partial^2 \hat{v}}{\partial \hat{t}^2} + \hat{c}\frac{\partial \hat{v}}{\partial \hat{t}} + \frac{\partial^4 \hat{v}}{\partial \hat{s}^4} + \frac{v_0^2}{l^2}\left(\frac{\partial^2 \hat{v}}{\partial \hat{s}^2}\right)^3 + 4\frac{v_0^2}{l^2}\frac{\partial \hat{v}}{\partial \hat{s}}\frac{\partial^2 \hat{v}}{\partial \hat{s}^2}\frac{\partial^3 \hat{v}}{\partial \hat{s}^3}\\&+ \frac{v_0^2}{l^2}\left(\frac{\partial \hat{v}}{\partial \hat{s}}\right)^2 \frac{\partial^4 \hat{v}}{\partial \hat{s}^4} + \frac{1}{2}\frac{v_0^2}{l^2}\frac{\partial \hat{v}}{\partial \hat{s}}\frac{\partial^2}{\partial \hat{t}^2}\int_0^{\hat{s}} \left(\frac{\partial \hat{v}}{\partial \hat{s}}\right)^2 \mathrm{d}\hat{s}\\&+ \frac{1}{2}\frac{v_0^2}{l^2}\frac{\partial^2 \hat{v}}{\partial \hat{s}^2}\int_1^{\hat{s}} \frac{\partial^2}{\partial \hat{t}^2}\int_0^{\hat{s}} \left(\frac{\partial \hat{v}}{\partial \hat{s}}\right)^2 \mathrm{d}\hat{s}\mathrm{d}\hat{s}\\&+ \frac{l^2}{EI}\frac{\partial^2 \hat{v}}{\partial \hat{s}^2}\int_1^{\hat{s}} F_1(t)\delta(\hat{s}-1)\mathrm{d}\hat{s}\\&+ \frac{3}{2}\frac{v_0^2}{EI}\left(\frac{\partial \hat{v}}{\partial \hat{s}}\right)^2 \frac{\partial^2 \hat{v}}{\partial \hat{s}^2}\int_1^{\hat{s}} F_1(t)\delta(\hat{s}-1)\mathrm{d}\hat{s}\\&= \frac{l^3}{v_0 EI}F_2(t)\delta(\hat{s}-1)\end{aligned} \tag{5}$$

The external nonconservative forces acting on the beam due to the interaction between the current loop and the external magnetic field can be formulated using the Lorentz force model

$$\vec{F}(t) = i(t)\int \mathrm{d}\vec{l}\ \mathrm{x}\ \vec{B}, \tag{6}$$

where $i(t)$ represents the current passing through the integrated loop and $\mathrm{d}\vec{l}$ represents the length vector associated with a differential element of the loop. Assuming the width of the current loop to be g, the Lorentz force model provides the following approximation for the external non-conservative force:

$$\begin{aligned}\vec{F}(t) &= F_1(t)\mathbf{i} + F_2(t)\mathbf{j}\\&= i(t)gB(\cos\alpha\mathbf{i} + \sin\alpha\mathbf{j}).\end{aligned} \tag{7}$$

The complex distributed parameter model developed earlier can be reduced into a lumped mass analog by decomposing the transverse displacement $\hat{v}$ into its spatial and temporal components

$$\hat{v}(\hat{s},\hat{t}) = \sum_{i=0}^{\infty} w_i(\hat{t})\Psi_i(\hat{s}), \tag{8}$$

and projecting the result onto the first mode shape of the system. This yields the final, lumped-parameter equation of motion for the system, given by:

$$\begin{aligned}&z'' + \epsilon\bar{c}z' + \left[1 + \epsilon\lambda_1 i(\tau)\right]z + \left[\epsilon k_3 + \epsilon\lambda_3 i(\tau)\right]z^3\\&\quad + \epsilon\beta(zz'^2 + z^2 z'') = \epsilon\eta_1 i(\tau).\end{aligned} \tag{9}$$

The system parameters included here are defined in Table 1.

While the use of the Lorentz force model introduced above ultimately leads to a relationship between the voltage input and the output displacement,

Table 1: Definitions of the nondimensional parameters used in Eqn. (9).

$$z = w(\hat{t})$$

$$\omega_0^2 = \int_0^1 \Psi\Psi^{iv}\mathrm{d}\hat{s}$$

$$\epsilon\bar{c} = \frac{\hat{c}}{\omega_0}$$

$$\tau = \omega_0\hat{t}$$

$$(\bullet)' = \frac{\partial(\bullet)}{\partial\tau}$$

$$\hat{\omega} = \omega T$$

$$\Omega = \frac{\hat{\omega}}{\omega_0}$$

$$\epsilon k_3 = \frac{v_0^2}{l^2\omega_0^2}\left(4\int_0^1 \Psi\Psi'\Psi''\Psi'''\mathrm{d}\hat{s} + \int_0^1 \Psi\Psi''^3\mathrm{d}\hat{s} + \int_0^1 \Psi\Psi'^2\Psi^{iv}\mathrm{d}\hat{s}\right)$$

$$\epsilon\lambda_1 = \frac{gBl^2\cos\alpha}{EI\omega_0^2}\left(\int_0^1 \Psi\Psi''\int_1^{\hat{s}}\delta(\hat{s}-1)\mathrm{d}\hat{s}\mathrm{d}\hat{s}\right)$$

$$\epsilon\lambda_3 = \frac{3v_0^2gB\cos\alpha}{2EI\omega_0^2}\int_0^1 \Psi\Psi'^2\Psi'''\int_1^{\hat{s}}\delta(\hat{s}-1)\mathrm{d}\hat{s}\mathrm{d}\hat{s}$$

$$\epsilon\beta = \frac{v_0^2}{l^2}\left(\int_0^1 \Psi\Psi''\int_1^{\hat{s}}\int_0^{\hat{s}}\Psi'^2\mathrm{d}\hat{s}\mathrm{d}\hat{s}\mathrm{d}\hat{s} + \int_0^1 \Psi\Psi'\int_0^{\hat{s}}\Psi'^2\mathrm{d}\hat{s}\mathrm{d}\hat{s}\right)$$

$$\epsilon\eta_1 = \frac{gBl^3\sin\alpha}{EIv_0\omega_0^2}\int_0^1 \Psi\delta(\hat{s}-1)\mathrm{d}\hat{s}$$

the procedure fails to capture the relationship between the displacement and the induced electromotive force (emf) associated with the system. The generation of a response-dependent emf is the principal motivation behind using an electromagnetically actuated microcantilever system and this can be derived through a direct application of Faraday's law [31]. The magnetic flux $\Phi(t)$ through any surface (with a normal direction denoted by $\hat{n}$) is given by:

$$\begin{aligned}\Phi(t) &= \iint_S (\vec{B}\cdot\hat{n})\mathrm{d}S \\ &= \iint_S B\sin\alpha\sin\psi\mathrm{d}S + \iint_S B\cos\alpha\cos\psi\mathrm{d}S.\end{aligned} \tag{10}$$

Applying third-order Taylor series approximations and nondimensionalizing the equations, as in Eqn. (4), yields an expression for the flux through the surface. Using modal projection techniques as before, the lumped-mass approximation of the flux is given by:

$$\begin{aligned}\Phi(\hat{t}) = &\left[Bg\sin\alpha v_0\int_0^1\Psi\int_0^1\Psi'\mathrm{d}\hat{s}\mathrm{d}\hat{s}\right]z \\ &+ Bg\cos\alpha l\int_0^1\Psi\mathrm{d}\hat{s} \\ &+ \left[\frac{Bg\cos\alpha v_0^2}{2l}\int_0^1\Psi\int_0^1\Psi'^2\mathrm{d}\hat{s}\mathrm{d}\hat{s}\right]z^2.\end{aligned} \tag{11}$$

The induced emf on the beam, as given by Faraday's law is:

$$\begin{aligned}V_{emf} &= -\frac{\partial\Phi(t)}{\partial t} \\ &= -\frac{1}{T}\frac{\partial\Phi(\hat{t})}{\partial\hat{t}}.\end{aligned} \tag{12}$$

Accordingly, the lumped-mass approximation for the induced emf is given by:

$$\begin{aligned}V_{emf} = &-\left(\frac{Bg\sin\alpha v_0}{T}\int_0^1\Psi\int_0^1\Psi'\mathrm{d}\hat{s}\mathrm{d}\hat{s}\right)\dot{z} \\ &-\left(\frac{Bg\cos\alpha v_0^2}{lT}\int_0^1\Psi\int_0^1\Psi'^2\mathrm{d}\hat{s}\mathrm{d}\hat{s}\right)z\dot{z}\end{aligned} \tag{13}$$

A brief examination of the equation of motion [Eqn. (9)] and the expression for induced emf [Eqn. (13)] reveals that when the magnetic field is oriented in the vertical direction ($\alpha = 90°$), the system is directly excited and the induced emf has a purely linear relationship with the response. If the magnetic field is oriented in the horizontal direction ($\alpha = 0°$), the system has a pure parametric excitation and a nonlinear relationship between the induced emf and the response. Intermediate orientations feature a complex relationship between the parameters and considerably richer dynamics.

3. A Single Input - Single Output Mass Sensor Based on a Globally-Coupled Array of Electromagnetically-Actuated Microcantilevers:

A schematic diagram of a representative array of electromagnetically actuated microcantilevers is shown in Fig. 3. The resonators are spaced such that there is negligible elastic coupling between the resonators. The cantilevers in the array are frequency mistuned by varying their lengths. A single wire loop connects all of the resonators in series and the device is placed in an external magnetic field. As a current

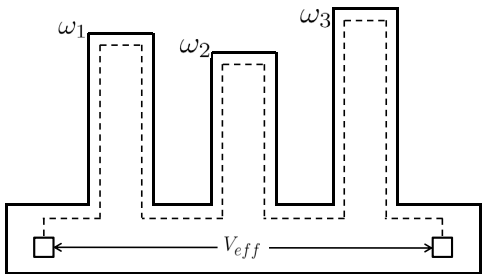

Figure 3: Schematic diagram of an array of electromagnetically-actuated microcantilevers with an integrated current loop used to realize global coupling. Note that V_{eff} is the voltage that is supplied to the array from the source after accounting for the induced electromotive force.

is supplied through the loop, the Lorentz force causes the device to move. The induced emf due to the motion of the resonator opposes the applied emf and is sensed through the same loop. This frequency dependent behavior from each of the resonator therefore affects the behavior of all the other cantilevers. This kind of a coupling is referred to here as global electromagnetic coupling. Note that by providing input to the loop and sensing the effective voltage across the loop, the device can operate as a single input - single output system.

For present purposes, a linear variant of the model developed in the preceding section is considered. Specifically, the model considered here is expanded from Eqn. (9) after accounting for the induced emf in the system. To simplify analysis, the angular orientation of the magnetic field α is assumed to be $\pi/2$ so that the parametric effects are negligible and direct excitation effects are dominant. Accordingly, the equation of motion is given by:

$$z'' + \epsilon(\bar{c} - \alpha_2)z' + z = \epsilon\eta_1 i(\tau), \tag{14}$$

where z, $\epsilon\bar{c}$, $\epsilon\lambda_1$ and $\epsilon\eta_1$ have been defined as in Table 1 and

$$\epsilon\alpha_2 = -\frac{(Bg)^2 \sin^2\alpha T}{Z\omega_0\rho A}\int_0^1 \Psi \int_0^1 \Psi' \mathrm{d}\hat{s}\mathrm{d}\hat{s}. \tag{15}$$

Note that the parameter Z included in these terms is defined to be the effective impedance of the current loop in the resonators. Extending the model to an array of cantilevers, the equation of motion is transformed to the following:

$$\mathbf{M}\mathbf{z}'' + \mathbf{C}\mathbf{z}' + \mathbf{K}\mathbf{z} = \bar{\boldsymbol{\eta}}_\mathbf{1}\cos\Omega\tau. \tag{16}$$

Here, $\mathbf{M}$ and $\mathbf{K}$ are diagonal matrices containing the mass elements and the stiffness elements m_i and k_i respectively, and $\mathbf{z}$ and $\bar{\boldsymbol{\eta}}_\mathbf{1}$ are the vectors containing the displacement (z_i) and amplitude of the forcing term ($\bar{\eta}_i$) in each of the resonators respectively. Since the expressions are normalized, the mass matrix is an identity matrix. The damping matrix $\mathbf{C}$ is given by:

$$\mathbf{C}_{nxn} = \epsilon\begin{bmatrix} \bar{c}_1 - \alpha_2 & -\alpha_2 & \dots & -\alpha_2 \\ -\alpha_2 & \bar{c}_2 - \alpha_2 & \dots & -\alpha_2 \\ \vdots & \vdots & \ddots & \vdots \\ -\alpha_2 & -\alpha_2 & \dots & \bar{c}_n - \alpha_2 \end{bmatrix}. \tag{17}$$

Table 2: Definitions of the nondimensional parameters used in the equation of motion of an array of coupled, electromagnetically-actuated microcantilevers.

$$\hat{s}_i = \frac{s}{l_i}$$

$$T = \sqrt{\frac{\rho A_{nom} l_{nom}^4}{EI_{nom}}}$$

$$\omega_0^2 = \int_0^1 \Psi_1 \Psi_1^{iv} \mathrm{d}\hat{s}$$

$$\hat{c}_i = \frac{c_i T}{\rho A_i}$$

$$\epsilon\bar{c}_i = \frac{\hat{c}_i}{\omega_0}$$

$$k_i = \frac{EI_i T^2}{\rho A_i l_i^4 \omega_0^2}\int_0^1 \Psi_i \Psi_i^{iv} \mathrm{d}\hat{s}$$

$$\tau = \omega_0 \hat{t}$$

$$(\bullet)' = \frac{\partial(\bullet)}{\partial\tau}$$

$$\hat{\omega} = \omega T$$

$$\Omega = \frac{\hat{\omega}}{\omega_0}$$

$$\epsilon(\bar{\eta}_1)_i = \frac{V g_i B T^2 \sin\alpha}{Z\rho A_i l_i v_0 \omega_0^2}\int_0^1 \Psi_i \delta(\hat{s}_i - 1)\mathrm{d}\hat{s}_i$$

$$\epsilon(\alpha_2)_i = -\frac{(Bg_i)^2(\sin^2\alpha)T}{Z\omega_0\rho A_i}\int_0^1 \Psi_i \int_0^1 \Psi_i' \mathrm{d}\hat{s}_i \mathrm{d}\hat{s}_i$$

The parameters in the expression are defined in Table 2. Note that in both Table 2 and all subsequent analysis, $(\bullet)_{nom}$ refers to the properties of a nominal resonator and $(\bullet)_i$ refers to the properties of i^{th} resonator.

3.1 Analysis:

The frequency response characteristics of an array of electromagnetically-actuated microcantilevers can be found using common techniques for the analysis of linear vibrating systems [32]. To this end, a steady-state solution for Eqn. (16) of the following form is assumed:

$$\mathbf{z}(\tau) = \mathbf{z}(i\Omega)e^{i\Omega\tau}, \tag{18}$$

where $\mathbf{z}(i\Omega)$ is the amplitude vector given as a function of the normalized excitation frequency Ω. Substituting in Eqn. (16) and solving for the amplitude vector yields,

$$\mathbf{z}(i\Omega) = \mathbf{Y}^{-1}(i\Omega)\bar{\boldsymbol{\eta}}_{\mathbf{1}}, \tag{19}$$

where, $\mathbf{Y}(i\Omega)$ is the system's impedance matrix which is given by

$$\mathbf{Y}(i\Omega) = -\Omega^2\mathbf{M} + i\Omega\mathbf{C} + \mathbf{K}. \tag{20}$$

The n^{th} component of the vector $\mathbf{z}(i\Omega)$, that is, $[\mathbf{z}(i\Omega)]_n$ represents the complex amplitude of the n^{th} cantilever in the array. Thus, the velocity of n^{th} cantilever is given by $i\Omega[\mathbf{z}(i\Omega)]_n$. Accordingly, the output voltage measured across the terminals (Fig. 3) is given by

$$V_o = V_{in} + \sum_{p=1}^{N} \alpha_2 i\Omega[\mathbf{z}(i\Omega)]_p. \tag{21}$$

To study the behavior of the system, the output voltage measured across the two terminals is plotted as a function of the normalized excitation frequency. The system considered for analysis is a 3-cantilever array. For initial analysis, the beam dimensions are assumed to be comparable to the device presented in [9]. The dimensions and the material properties are listed in Table 3. Note that the first cantilever is assumed to be the nominal beam and the lengths of other two cantilevers are modified from the length of the first beam to introduce frequency mistuning in the system. The width and thickness of all the cantilevers are identical.

Figure 4 shows the normalized output voltage V_o plotted against the normalized excitation frequency. The frequency response shows three distinct antiresonances in the response, corresponding to each of the cantilever's resonance frequencies. Thus, by measuring the output voltage across the two terminals, all the three resonance frequencies can be captured. This would imply that by functionalizing the three beams to detect three different analytes, this system can be used as a single input - single output, multi-analyte sensor [17].

Table 3: Dimensions and material properties used to study the frequency response of a representative electromagnetically-actuated microcantilever system.

Physical Parameter	Value
Length of Beam 1	162 μm
Length of Beam 2	157 μm
Length of Beam 3	167 μm
Width	23.5 μm
Thickness	250 nm
Young's Modulus (E)	159 GPa
Mass Density (ρ)	2330 kg/m^3
Magnetic Field Strength (B)	1 T
Quality Factor (Q)	500

3.2 Design Considerations:

The factors that need to be considered when designing a mass sensor based on an array of electromagnetically actuated cantilevers are the extent of mechanical coupling between the resonators, the spacing of the individual resonance frequencies and the quality factors of the individual resonators in the array. Mechanical coupling between the resonators typically occurs when the beams are closely spaced and affects the frequency response of the device. The mass sensor described herein aims to take advantage of only the electromagnetic coupling and hence the resonators need to be spaced to avoid mechanical coupling effects. This, in addition to ensuring adequate spacing of the individual resonance frequencies, also helps to ensure that the adsorption of a target analyte affects only the natural frequency of the mass-loaded resonator and that shifts in the aforementioned resonance are easily detectable.

The quality factor of the individual resonators affects the number of resonators that can be accommodated in a given frequency bandwidth. For the device described herein, the frequency bandwidth is the difference between the highest and the lowest resonance frequencies of the individual resonators in the system.

Figure 5 shows the theoretical frequency response of the resonator array before and after the addition of analyte on the resonator with the lowest frequency. A mass addition of 1% of the mass of the

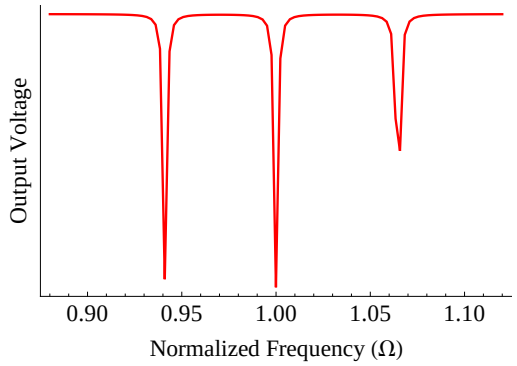

Figure 4: The measured normalized output voltage V_o (arbitrary units) of an electromagnetically-actuated microcantilever array plotted against the normalized excitation frequency Ω for the parameter values shown in Table 3. The response shows three distinct antiresonances corresponding to the coupled natural frequencies of the system.

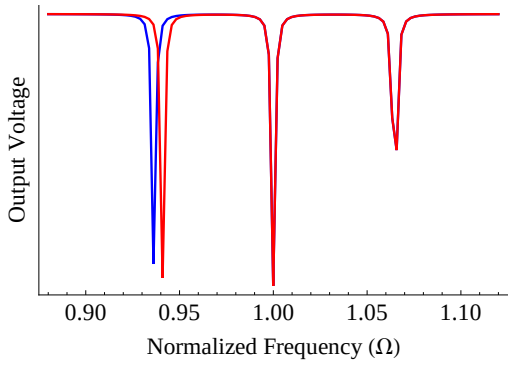

Figure 5: The output normalized voltage V_o (arbitrary units) of an electromagnetically-actuated microcantilever array plotted against the normalized excitation frequency Ω for the parameter values shown in Table 3, with and without added mass. The red curve corresponds to the sensor without the added mass, while the blue curve corresponds to the sensor with the added mass on the third cantilever (the cantilever with the lowest uncoupled natural frequency). The natural frequency of the loaded cantilever is altered significantly while the resonant frequencies of the other cantilevers are largely unchanged, indicating that this sensor can be used as a single-input and single-output device capable of detecting multiple analytes.

cantilever is assumed. The red curve corresponds to the response of the sensor without the added mass while the blue curve corresponds to the sensor with the added mass. Note that the natural frequency of the loaded cantilever is altered significantly, while the resonant frequencies of the other cantilevers are largely unchanged. Thus, by tracking the resonance frequency shifts of individual resonators through the common output, this technique can be used for the detection of multiple analytes.

3.3 Sensor Metrics:

The minimum detectable mass or mass sensitivity is an important metric used to compare the effectiveness of a mass sensor against other comparable platforms. The mass sensitivity of a single-degree-of-freedom sensor is a function of mass responsivity and frequency resolution, and is given by [33]:

$$\delta m \approx R^{-1}\delta\omega, \tag{22}$$

where δm is the mass sensitivity of the sensor, $\delta\omega$ is the frequency resolution of the system and R is the mass responsivity of the sensor.

Using a similar procedure, the mass sensitivity of a multi-degree-of-freedom sensor can be expressed as in [34]:

$$\mathbf{\Delta m} \approx \mathbf{R}^{-1}\mathbf{\Delta\omega}, \tag{23}$$

where $\mathbf{\Delta m}$ is a vector of mass sensitivities associated with each of the microresonator, $\mathbf{R}$ is the responsivity matrix associated with the sensor and $\mathbf{\Delta\omega}$ is the vector of the frequency resolutions corresponding to each of the resonators.

In a single-degree-of-freedom sensor, the mass responsivity is given by

$$R = \frac{\partial\omega_n}{\partial m_{eff}}, \tag{24}$$

where ω_n is the natural frequency of the sensor and m_{eff} is the effective mass of the system, accounting for the added mass due to the adsorption of the analyte on the functionalized sensor surface. However, in the coupled multi-degree-of-freedom sensor, when mass adsorbs on one of the resonators, the resonance frequencies of all the resonators are modified. Therefore, the responsivity matrix is square and of order n (the same as the number of resonators). Hence, the mass responsivity of the sensor is a matrix, defined by

$$\mathbf{R}_{ij} = \frac{\partial\omega_i}{\partial m_j}, \tag{25}$$

where ω_i is the natural frequency of the i^{th} resonator and m_j is the effective mass of the j^{th} resonator. In the particular case of electromagnetically-actuated microresonators, the coupling is dissipative

and hence, the damping matrix cannot be ignored. Therefore, in Eqn. (25), ω_i refers to the damped natural frequency of the system. A sensor with strong mode localization would have a diagonally dominant responsivity matrix [34].

For illustrative purposes, the device described in Table 3 is considered here. The undamped and uncoupled natural frequencies of the three resonators are 12.712 kHz, 13.534 kHz and 11.962 kHz respectively. In order to determine the responsivity of the sensor, the damped, coupled natural frequencies of the system are needed. These frequencies are obtained by equating Eqn. (20) to zero and solving for nontrivial solutions, that is,

$$|\mathbf{Y}(i\Omega)| = 0. \tag{26}$$

Obtaining the damped natural frequencies symbolically and using the result in Eqn. (25) yields the responsivity matrix for the system:

$$\mathbf{R}_{ij} = \begin{bmatrix} 18 & 0.77 \text{ x } 10^{-12} & 5.58 \text{ x } 10^{-12} \\ 2.08 \text{ x } 10^{-12} & 19.78 & 0.42 \text{ x } 10^{-12} \\ 3.78 \text{ x } 10^{-12} & 1.2 \text{ x } 10^{-12} & 16.44 \end{bmatrix} \frac{Hz}{pg}. \tag{27}$$

From Eqn. (27), it can be seen that, the diagonal elements are much larger than the off-diagonal elements. This implies that a change in the natural frequency of the i^{th} resonator as a result of added mass on the i^{th} resonator is much higher than the change caused due to the adsorption of mass on the other resonators. Therefore, by functionalizing each of the cantilevers to detect a different analyte and by detecting a given resonator's frequency shift, one can quickly identify the given analyte.

The above analysis has clearly shown that the proposed sensing technique is a viable method for mass sensing. Building on these results, current efforts are aimed at towards the experimental realization of such a sensor. This includes the design and fabrication of these devices, design of an associated electrical measurement setup, characterization of the sensor's frequency response behavior both optically and electrically, device functionalization and proof-of-concept mass sensing experiments.

4. Isolated Electromagnetically-Actuated Microbeam Oscillators:

As a first step to understand the dynamics of an array of electromagnetically-actuated oscillators, the dynamics of a single oscillator needs to be thoroughly examined. To this end, this section deals with the dynamics of an isolated microbeam system. An analysis

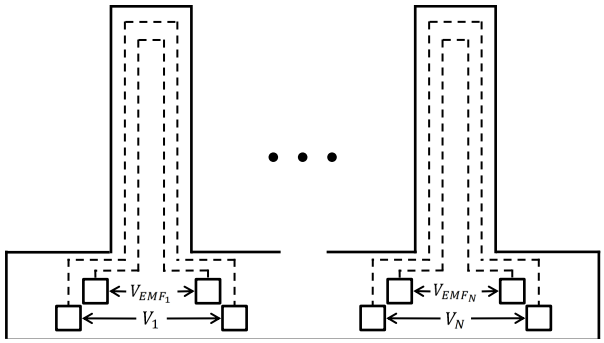

Figure 6: Schematic diagram of an array of electromagnetically-actuated microcantilevers oscillators. Note that each microcantilever has two current loops: one for actuation and one for sensing. The voltages applied to the device for actuation are of the form $V_i = V_{ci} + \sum_{i=1}^{N} G_{ci} G_i V_{emf_i}$ and the sensed voltage is V_{emf_i}, where subscript denotes the corresponding microbeam.

of the equation of motion for a single microbeam oscillator provides insight on the effect of various system parameters on the system's dynamics and can be easily extended to coupled arrays. Figure 6 shows a schematic diagram of the device considered here. The device is a minor modification from the device shown in Fig. 3, with each beam having independent actuation and sensing loops. With the introduction of feedback in the system, the beam actuation can be made to be dependent on the sensed emf, thus making the array of microbeams self-sustaining. For the case of a single microbeam, a positive feedback control law of the following form is considered. Here,

$$i(\tau) = \frac{V_c}{R} \tag{28}$$

is the current in the actuation loop and

$$V_c = GV_{emf} - KG^3 V_{emf}^3 \tag{29}$$

is the voltage supplied by the controller. The parameters of the control law are the resistance of the actuation loop R, the gain applied to the emf G, and a parameter used to control the amplitude of oscillator K. The lumped mass approximation of the emf in terms of the nondimensional displacement is

$$\begin{aligned} V_{emf} &= \kappa_1 z' + \kappa_2 z z', \\ \kappa_1 &= -\frac{Bg \sin\alpha v_0}{T\omega_0} \int_0^1 \Psi \int_0^1 \Psi' \mathrm{d}\hat{s}\mathrm{d}\hat{s}, \\ \kappa_2 &= -\frac{Bg \cos\alpha v_0^2}{lT\omega_0} \int_0^1 \Psi \int_0^1 \Psi'^2 \mathrm{d}\hat{s}\mathrm{d}\hat{s}. \end{aligned} \tag{30}$$

The above control law, in conjunction with Eqn. (9), yields the equation of motion for a microbeam oscillator (truncated to contain up to third-order terms):

$$z'' + (\epsilon\bar{c} - \frac{G\kappa_1\epsilon\eta_1}{R})z' + z + \frac{G(\kappa_1\epsilon\lambda_1 - \kappa_2\epsilon\eta_1)}{R}zz' + \epsilon k_3 z^3 + \epsilon\beta(zz'^2 + z^2z'') + \frac{G\kappa_2\epsilon\lambda_1}{R}z^2z' + \frac{KG^3\kappa_1^3\epsilon\eta_1}{R}z'^3 = 0. \tag{31}$$

Equation (31) can be rewritten in the form of a Lienard Equation, from which the existence of a stable limit cycle can be studied:

$$z'' + f(z, z')z' + g(z) = 0, \tag{32}$$

where

$$f(z, z') = \frac{\epsilon\bar{c} - \gamma_1 + \gamma_5 z + \gamma_3 z^2 + \epsilon\beta zz' + \frac{8\gamma_2}{3}z'^2}{1 + \epsilon\beta z^2}, \quad g(z) = \frac{z + \epsilon k_3 z^3}{1 + \epsilon\beta z^2}. \tag{33}$$

The parameters in Eqn. (33) are expressed in Table 4.

Table 4: Definitions of the parameters used in Eqn. (32).

$$\gamma_1 = \frac{G\kappa_1\epsilon\eta_1}{R}$$
$$\gamma_2 = \frac{3G^3K\kappa_1^3\epsilon\eta_1}{8R}$$
$$\gamma_3 = \frac{G\kappa_2\epsilon\lambda_1}{8R}$$
$$\gamma_4 = \frac{3\epsilon k_3}{8} - \frac{\epsilon\beta}{4}$$
$$\gamma_5 = \frac{G(\kappa_1\epsilon\lambda_1 - \kappa_2\epsilon\eta_1)}{R}$$

The conditions under which at least one stable periodic solution exists are given by [35]:

1. There exists $a > 0$ such that $f(z, z') > 0$, when $z^2 + z'^2 > a^2$;.
2. $f(0, 0) < 0$;
3. $g(0) = 0$, $g(z) > 0$ when $z > 0$, and $g(z) < 0$ when $z < 0$;
4. $G(z) = \int_z^0 g(u)\,du \to \infty$ as $z \to \infty$.

The first condition is satisfied as long as $8\gamma_2/3 + \gamma_3 > \epsilon\beta$. The second condition is true if $\gamma_1 > \epsilon\bar{c}$. The third and fourth conditions are satisfied as long as ϵk_3 and $\epsilon\beta$ are positive. While this method guarantees that at least one stable period solution exists, it does not allow for any insight into the type of solution. Assuming that G and K are not large, the system can be considered to be a weakly nonlinear oscillator, and therefore, the method of averaging can be used [36]. Introducing a coordinate transformation of the form

$$z(\tau) = a(\tau)\cos[\tau + \phi(\tau)], \quad z'(\tau) = -a(\tau)\sin[\tau + \phi(\tau)] \tag{34}$$

renders slow flow equations given by:

$$a'(\tau) = \frac{1}{2}(\gamma_1 - \epsilon\bar{c})a - (\gamma_2 + \gamma_3)a^3 + O(\epsilon^2), \quad \phi'(\tau) = \gamma_4 a^2 + O(\epsilon^2). \tag{35}$$

This results in a steady-state response given by

$$a = \sqrt{\frac{\frac{1}{2}a_0^2\sigma_1}{\sigma_2 + \left(\frac{1}{2}\sigma_1 - \sigma_2\right)e^{-\sigma_1\tau}}}, \quad \phi = \phi_0 + \frac{\gamma_4}{2(\gamma_2 + \gamma_3)}\ln[\frac{2\sigma_2(e^{\sigma_1\tau} - 1) + \sigma_1}{\sigma_1}], \tag{36}$$

where

$$\sigma_1 = \gamma_1 - \epsilon\bar{c}, \quad \sigma_2 = a_0^2(\gamma_2 + \gamma_3),$$

and a_0 and ϕ_0 are the initial amplitude and phase. Equation (36) clearly shows that in order to have a stable limit cycle, $\gamma_1 > \epsilon\bar{c}$ and $a_0 > 0$. Under these conditions, the steady-state solutions are given by:

$$\hat{a} = \lim_{\tau\to\infty} a(\tau) = \sqrt{\frac{\gamma_1 - \epsilon\bar{c}}{2(\gamma_2 + \gamma_3)}}, \quad \hat{\phi} = \lim_{\tau\to\infty} \phi(\tau) = \phi_0 + \frac{\gamma_4}{\gamma_2 + \gamma_3}\ln[\frac{a_0}{\hat{a}}] + \gamma_4\hat{a}^2\tau. \tag{37}$$

The steady-state amplitude $\hat{a}$ can be used to generate a bifurcation diagram of the system, which for the parameters in Table 3 and $\alpha = \pi/2$, is shown in Fig. 7. Note that the trivial solution is the only solution when $\gamma_1 < \epsilon\bar{c}$.

The equation for the steady-state phase shows that the nonlinearities in the system cause the frequency to be increased relative to the undamped natural frequency and that there is a phase shift due to the initial amplitude. The frequency shift can

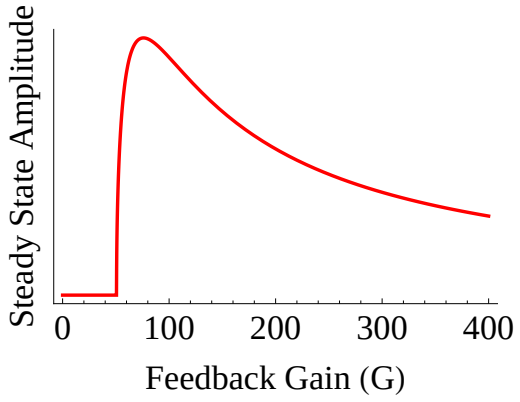

Figure 7: Bifurcation diagram of the steady-state amplitude (arbitrary units) for the parameters in Table 3 and $\alpha = \pi/2$.

be compensated for by adding a constant value to the feedback, but then the Lienard Equation form of the equation of motion would violate the conditions under which at least one stable periodic solution must exist. The averaged equations highlights two other important features: First, K can be used to control the steady-state amplitude, but K also could be zero and still have stable oscillations; and second, assuming all the parameters in γ_1 are fixed except for G and $\alpha \neq \pi/2$, that G can be used to control how quickly the system settles to the limit cycle.

5. Coupled Arrays of Electromagnetically-Actuated Microbeam Oscillators:

The model for two coupled microbeam oscillators can be developed by modifying the model for a single microbeam oscillator. Here, a subscript denotes the quantity associated with a given microbeam and the control laws for the coupled microbeam oscillators are given by:

$$\begin{aligned} i_1(\tau) &= \frac{V_{c1} + G_c G V_{emf2}}{R}, \\ i_2(\tau) &= \frac{V_{c2} + G_c G V_{emf1}}{R}. \end{aligned} \tag{38}$$

Note that all other quantities not defined explicitly are the same as in the case of a single microbeam system. Assuming that the microbeams are identical except for a small frequency mistuning δ, the averaged equations for the coupled system are given by:

$$\begin{aligned} a_1'(\tau) &= \frac{1}{2}(\gamma_1 - \epsilon\bar{c})a_1 - (\gamma_2 + \gamma_3)a_1^3 \\ &\quad - G_c\gamma_3 a_1 a_2^2 \cos(2\psi) + \frac{1}{2}G_c\gamma_1 a_2 \cos(\psi) + O(\epsilon^2), \\ a_2'(\tau) &= \frac{1}{2}(\gamma_1 - \epsilon\bar{c})a_2 - (\gamma_2 + \gamma_3)a_2^3 \\ &\quad - G_c\gamma_3 a_1^2 a_2 \cos(2\psi) + \frac{1}{2}G_c\gamma_1 a_1 \cos(\psi) + O(\epsilon^2), \\ \psi'(\tau) &= -\frac{1}{2}\delta + \gamma_4(a_1^2 - a_2^2) + G_c\gamma_3(a_1^2 + a_2^2)\sin(2\psi) \\ &\quad - \frac{1}{2}G_c\gamma_1\left(\frac{a_1}{a_2} + \frac{a_2}{a_1}\right)\sin(\psi) + O(\epsilon^2), \end{aligned} \tag{39}$$

where $\psi = \phi_1 - \phi_2$. If the magnetic field is assumed to be oriented vertically, then $\gamma_3 = 0$ and the averaged equations reduce to a set of equations which have been previously studied [23–25]. Solutions to Eqn. (39) can be either be symmetric and phase locked (amplitudes are equal and ψ is constant), asymmetric (amplitudes are not equal), exhibit phase drift (ψ varies with time), or quenched (amplitudes are zero). Prior work has shown that the asymmetric solution is unstable [23]. Accordingly the conditions under which the symmetric and phase locked solution exists and is stable are the only ones of interest here, as this is the only state that is synchronized. The stable symmetric and phase locked solution is governed by:

$$\begin{aligned} a^2 &= \frac{2\,(\gamma_1 - \hat{c}) + \sqrt{4G_c^2\gamma_1^2 - \delta^2}}{4\gamma_2}, \\ \psi &= -\sin^{-1}\left(\frac{\delta}{2G_c\gamma_1}\right), G_c > 0, \\ \psi &= \sin^{-1}\left(\frac{\delta}{2G_c\gamma_1}\right) - \pi, G_c < 0, \end{aligned} \tag{40}$$

where $a = a_1 = a_2$. This solution is stable everywhere when it exists. Thus, in the simplest coupled oscillator array, the array is capable of producing a single state, or pattern. The limitation with this result is that the averaged equations are only valid when the system is weakly nonlinear, or when G, K, G_c and δ are small. So two arbitrary beams can not necessarily be synchronized (i.e. δ can be large or small) by increasing G_c. As δ increases however, other forms of synchronization are possible [25].

For arrays with a larger numbers of oscillators, it is possible that more than one pattern can be stable and that the pattern the array converges to is dependent on the initial conditions. As was shown in [21], with three oscillators it is possible to have two different synchronization states. Mendelowitz, et al

considered a model of oscillators with and without amplitude dynamics. In the specific case they studied, the ability for the system to exhibit two different stable patterns was not lost when considering only phase dynamics, but amplitude dynamics had to be considered to determine the conditions under which the patterns could exist.

Direct applications of this preliminary research include mass sensing, electromagnetic signal processing and other areas where small shifts in frequency are directly exploitable for practical gain [30].

Acknowledgements: This effort was graciously supported by the National Science Foundation via Grant 0846385.

References:

[1] D. S. Greywall. Micromechanical RF filters excited by the Lorentz force. *Journal of Micromechanics and Microengineering*, 9(1):78–84, 1999.

[2] S. J. Martin, M. A. Butler, J. J. Spates, M. A. Mitchell, and W. K. Schubert. Flexural plate wave resonator excited with Lorentz forces. *Journal of Applied Physics*, 83(9):4589–4601, 1998.

[3] M. Schiffer, V. Laible, and E. Obermeier. Design and fabrication of 2D Lorentz force actuated micromirrors. In Proceedings of *The 2002 IEEE/LEOS International Conference on Optical MEMS*, 163–164, Lugano, Switzerland, 2002.

[4] S. C. Jun, X. M. H. Huang, J. Hone, C. A. Zorman, and M. Mehregany. Evaluation of 3C-SiC nanomechanical resonators using room temperature magnetomotive transduction. In Proceedings of *IEEE Sensors 2005: The 4th IEEE Conference on Sensors*, 1042–1045, Irvine, California, 2005.

[5] X. M. H. Huang, X. L. Feng, C. A. Zorman, M. Mehregany, and M. L. Roukes. VHF, UHF and microwave frequency nanomechanical resonators. *New Journal of Physics*, 7(247):1–15, 2005.

[6] M. V. Requa and K. L. Turner. Electromechanically driven and sensed parametric resonance in silicon microcantilevers. *Applied Physics Letters*, 88:263508, 2006.

[7] M. V. Requa. *Parametric Resonance in Microcantilevers for Applications in Mass Sensing*. PhD dissertation, University of California, 2006.

[8] M. V. Requa and K. L. Turner. Precise frequency estimation in a microelectromechanical parametric resonator. *Applied Physics Letters*, 90:173508, 2007.

[9] J. F. Rhoads. *Exploring and Exploiting Resonance in Coupled and/or Nonlinear Microelectromechanical Oscillators*. PhD dissertation, Michigan State Univeristy, 2007.

[10] F. D. Bannon III, J. R. Clark, and C. T.-C. Nguyen. High-Q HF microelectromechanical filters. *IEEE Journal of Solid-State Circuits*, 35(4):512–526, 2000.

[11] V. B. Chivukula and J. F. Rhoads. Microelectromechanical bandpass filters based on cyclic coupling architectures. *Journal of Sound and Vibration*, 329:4313–4332, 2010.

[12] E. Buks and M. L. Roukes. Electrically tunable collective response in a coupled micromechanical array. *Journal of Microelectromechanical Systems*, 11(6):802–807, 2002.

[13] M. Spletzer, A. Raman, R. Reifenberger, A. Q. Wu, and X. Xu. Biochemical mass detection using mode localization in microcantilever arrays. In Proceedings of *IMECE 2005: The 2005 ASME International Mechanical Engineering Congress and Exposition*, Orlando, Florida, 2005.

[14] M. Spletzer, A. Raman, H. Sumali, and J. P. Sullivan. Highly sensitive mass detection and identification using vibration localization in coupled microcantilever arrays. *Applied Physics Letters*, 92:114102, 2008.

[15] E. Gil-Santos, D. Ramos, A. Jana, M. Calleja, A. Raman, and J. Tamayo. Mass sensing based on deterministic and stochastic responses of elastically coupled nanocantilevers. *Nano Letters*, 9(12):4122–4127, 2009.

[16] J. F. Rhoads, B. E. DeMartini, S. W. Shaw, and K. L. Turner. A SISO, multi-analyte sensor based on a coupled microresonator array. In Proceedings of *IMECE 2006: The 2006 ASME International Mechanical Engineering Conference and Exposition*, Chicago, Illinois, 2006.

[17] B. E. DeMartini, J. F. Rhoads, M. A. Zielke, K. G. Owen, S. W. Shaw, and K. L. Turner. A single input-single output coupled microresonator array for the detection and identification of multiple analytes. *Applied Physics Letters*, 93:054102, 2008.

[18] F. C. Hoppensteadt and E. M. Izhikevich. Synchronization of MEMS resonators and mechanical neurocomputing. *IEEE Transactions on Circuits and Systems I: Fundamental Theory and Applications*, 48(2):133–138, 2001.

[19] C. T.-C. Nguyen. MEMS technology for timing and frequency control. *IEEE Transactions on Ultrasonics, Ferroelectrics, and Frequency Control*, 54(2):251–270, 2007.

[20] M. C. Cross, J. L. Rogers, R. Lifshitz, and A. Zumdieck. Synchronization by reactive coupling and nonlinear frequency pulling. *Physical Review E*, 73:036205, 2006.

[21] L. Mendelowitz, A. Verdugo, and R. Rand. Dynamics of three coupled limit cycle oscillators with application to artificial intelligence. *Communications in Nonlinear Science and Numerical Simulation*, 14:270–283, 2009.

[22] A. Pikovsky, M. Rosenblum, and J. Kurths. *Synchronization: A Universal Concept in Nonlinear Sciences*. Cambridge Nonlinear Science Series. Cambridge University Press, New York, 2001.

[23] D. G. Aronson, G. B. Ermentrout, and N. Kopell. Amplitude response of coupled oscillators. *Physica D*, 41:403–449, 1990.

[24] M. V. Ivanchenko, G. V. Osipov, V.D. Shalfeev, and J. Kurths. Synchronization of two non-scalar-coupled limit-cycle oscillators. *Physica D*, 189:8–30, 2004.

[25] A. P. Kuznetsov and J. P. Roman. Properties of synchronization in the systems of non-identical coupled van der Pol and van der Pol-Duffing oscillators: broadband synchronization. *Physica D*, 238(16):1499–1506, 2009.

[26] S. Y. Ha, T. Ha, and J. H. Kim. On the complete synchronization of the Kuramoto phase model. *Physica D*, 239:1692–1700, 2010.

[27] J. A. Acebron, L. L. Bonilla, C. J. Perez Vicente, F. Ritort, and R. Spigler. The Kuramoto model: A simple paradigm for synchronization phenomena. *Review of Modern Physics*, 77:137–185, 2005.

[28] M. Pandey, R. Rand, and A. Zehnder. Perturbation analysis of entrainment in a micromechanical limit cycle oscillator. *Communications in Nonlinear Science and Numerical Simulation*, 12(7):1291–1301, 2007.

[29] S. H. Strogatz. From Kuramoto to Crawford: Exploring the onset of synchronization in populations of coupled oscillators. *Physica D*, 143:1–20, 2000.

[30] P. Liao and R. A. York. A new phase-shifterless beam-scanning technique using arrays of coupled oscillators. *IEEE Transactions on Microwave Theory and Techniques*, 41(10):1810–1815, 1993.

[31] A. Matveyev. *Principles of Electrodynamics*. Reinhold Publishing Company, New York, 1966.

[32] L. Meirovitch. *Principles and Techniques of Vibrations*. Prentice Hall, Upper Saddle River, 1997.

[33] K. L. Ekinci, Y. T. Yang, and M. L. Roukes. Ultimate limits to inertial mass sensing based upon nanoelectromechanical systems. *Journal of Applied Physics*, 95(5):2682–2689, 2004.

[34] B. E. DeMartini. *Development of Nonlinear and Coupled Microelectromechanical Oscillators for Sensing Applications*. PhD dissertation, University of California, 2008.

[35] D. W. Jordan and P. Smith. *Nonlinear Ordinary Differential Equations*. Oxford Applied Mathematics and Computing Science Series. Oxford University Press, Oxford, 2nd edition, 1987.

[36] A. H. Nayfeh and D. T. Mook. *Nonlinear Oscillations*. Wiley-Interscience, 1995.